RSC Advances

ROYAL SOCIETY OF CHEMISTRY

www.rsc.org/advances

ZnO long fibers: large scale fabrication, precursor and the transformation process, microstructure and catalytic performance

Benxue Liu, Xuejun Lin, Xinqiang Wang, Luyi Zhu*, Guanghui Zhang, Dong Xu*

ABSTRACT: The development of effective and low-cost catalysts for the synthesis of chemical energy and photo-assistant eliminating pollution is of great importance to sustainable development of human society. This work designs a fibrous ZnO which was composed by the stacking of ZnO nanoparticles. Photocatalysis investigation demonstrated that the fibers possess higher catalytic ability compared to their powder counterparts . Meanwhile, the former was more suitable for application in continuous mode and simple separation operation. The ZnO fibers were fabricated through centrifugal-spinning a molecular precursor sol into gel fibers followed by heat treatment. The viscous sol was synthesized by concentrating a zinc citrate aqueous solution which was made from citric acid and ZnO powders. The formation mechanism of the organozinc sol was investigated by a series of characterizations on precursor solution, gel precursor and the decomposition of the gel precursor. The results indicate that zinc citrate monomers in precursor solution were assembled into multinuclear structure induced by solvent evaporation.

1.Introduction

Metal oxides represent one of the most important and widely employed categories of solid catalysts, either as active phases or supports. They are utilized both for their acid-base and redox properties and constitute the largest family of heterogeneous catalysts.[1] Among them, Zinc oxide (ZnO) has attracted a great deal of attention in recent years. ZnO is a typical amphoteric metal oxide as well as an II-VI group semiconductor with a band gap of 3.37 eV. Owning to reliable catalytic ability, a wide range of chemical reactions can occur by the participation of ZnO, such as photodegradation pollution,[2] biodiesel synthesis,[3] and the synthesis of specific chemical substances.[4, 5] Meanwhile, the metal oxide is also an indispensible catalytic support of Cu/ZnO catalysts.[6] With the synergistic effect of ZnO, the mixtures are effective catalysts for low-pressure methanol synthesis.

Through the ages, the main application forms of ZnO in chemical reaction are nanopowders. Generally, these powders are directly suspended in fluidized bed reactor. However, it brings about some limitations in practical applications, such as complicated separation or filtration steps after reaction, the problematic use of continuous flow systems, and particle aggregation or particle sintering in high temperature environment.[7] Depositing the nanostructure on solid support can achieve their homogeneous dispersion and maximum surface site availability. For example, compared with slurry ZnO system, immobilizing ZnO on glass plates can achieve application in continuous mode.[8] Impregnation of ZnO on NaX zeolite generates even higher photocatalytic activity as well as good reusable ability.[9] In this case, it is an effective approach to tackle the abovementioned problems. Nevertheless, it should be noted that the loading technology requires complicated procedure which increases the overall cost. The active phase would drain little by little as the reaction proceeding because of the weak bonding between matrix and catalysts.

Fibrous ZnO is another strategy to overcome the above drawbacks. The fibers are self-standing in reaction system which features good recycling ability, and low resistance to fluid. Since 2004,[10] ZnO fibers are first synthesized by electrospinning a mixed solution of zinc salts and polymers followed by heat treatment. In past ten years, various research about the fabrication method of ZnO fibers are reported.[11-17] Lin[13] has fabricated Ag-ZnO nanofibers and employed it in photodegradation of Rhodamine B. The results indicate that it has comparative photocatalytic ability compared with P25 nanoparticles-a commercial photocatalysts. Singh[17] has developed a strategy to fabricate mesoporous ZnO nanofiber mats. These fibers possess good reusable ability with effective ability to photodegrade naphthalene and anthracene dyes. Meantime, when nanostructure (i.e. nanoparticles) are assembled into mesostructure (i.e. nanocrystalline fibers), some novel properties are obtained. For example, choi[18] has found that mesoporosity and particle interactions in TiO_2 naonofibers can facilitate the charge transfer, which in turn increases the photocatalytic ability of the fibers.

Therefore, the excellent performances of fibrous materials in catalytic process inspire us to explore more economical and efficient way to construct such structure. In this paper, ZnO long fibers were fabricated by centrifugal-spinning an organozinc sol into gel fibers followed by heat treatment. Extrusion of spin dopes from spinneret through centrifuge force to gain fibers is a powerful and effective spinning technology.[19] The centrifugal-spinning allows a significant increase in yield of production. The fiber production rate has been shown to be over 1 g/min per nozzle in the lab scale units, this yield is higher than any lab scale electrospinning appatatus where typical systems operate at about 0.1 g/h.[20] In current work, a self-made centrifugal-spinning device was introduced. The spinnable sol was synthesized by concentrating a zinc citrate aqueous solution which was made from citric acid and ZnO powders. In this research, we devoted ourselves to studying how the zinc citrate monomers ploymerized into multinuclear molecule which makes the system performs high viscosity, and how the organic gel fibers decompose into inorganic crystalline fibers. Interestingly, citric acid is found that can form spinnable sol with many kinds of metal ions.[21-25] We consider that the investigation on the polymerization process of metal citrate complex induced by solvent evaporation can not only be beneficial to explore new materials through this method, but also is helpful for understanding the process of molecule self-assembly. The relationship between the microstructure of the fibers and its photocatalytic ability was preliminary investigated through degradation of methylene blue.

2. Experimental

2.1 Starting materials

Zinc oxide (ZnO, 99.0 %, Kermel), citric acid (CA, 99.5 %, Kermel), deionized water (18.2 MΩ), ammonia (25 %~28 %, Kermel)

2.2 Synthesis of ZnO fibers

10.00 g CA were dissolved in 100 ml deionized water. Designed amount of ZnO powders were added into the CA solution and magnetically stirred till the white ZnO powders dissolved completely. After that, appropriate amount (about 5~10 ml) of ammonia was added into the obtained transparent solution to adjusted the pH to a required value. The solution was stirred for another 2 h to attain chemical homogeneity. Then, it was concentrated into some viscous by the vacuum rotary evaporator at 60 ℃. The appropriate viscosity is about 24000 mPa•s measured by a rotary viscosimeter. The viscous transparent sol adaptive for spinning can be synthesized (Figure S1).

The spinnable sol was spun into ZnO precursor fibers using a self-made centrifugal-spinning device (Figure S1). The detailed spinning parameters are shown in Table S1. The precursor fibers were dried in a drying oven at 50 ℃ for 12 h and then put into a furnace for heat treatment. Based on thermal analysis results, the heat treatment schedule was established. A slow heating rate of 0.5 ℃/min up to 450 ℃ was expected to drive off the organics of the precursors gradually and completely. The second heating process with a higher heating rate of 2 ℃/min was up to the desired temperature. The fibers were held at the desired temperature for 2 h and then slowly cooled to room temperature in the furnace to obtain final products.

2.3 Measurements

The carbon nuclear magnetic resonance (^{13}C-NMR) spectra were recorded at 25 ℃ using Bruker advance 300 M spectrometer, the solvent was D_2O. The infrared (IR) spectra were recorded on a Nicolet 5DX-FTIR spectrometer using KBr pellet method in the range of 4000-375 cm^{-1}. The thermal behavior of the precursor fibers were studied by thermo gravimetric analysis (TG) and differential scanning calorimetric analysis (DSC) using SDT Q600 V8.3 Build 101 thermal analyzer instrument, ranging from room temperature to 800 ℃ at a heating rate of 10 ℃/min under air atmosphere. The X-ray diffraction (XRD) patterns for fibers sintered at different temperatures were collected on a Bruker AXSD8 Advance X-ray diffractometer with Cu Kα radiation using a graphite chromator. Diffraction peaks were recorder in the 10-90° (2θ) range with a step size of 0.02°. The morphologies and microstructures of the samples were characterized using Hitachi S-4800 scanning electron microscope (SEM) instrument. The N_2 adsorption/desorption isotherms of the fibers heat-treated at different temperatures and ZnO powders were measured at 77 K on a Quadrasorb-SI instrument. Before the measurement, all samples were degassed at 200 ℃ for at least 8 h. The photocurrent were measured using a CHI660D electrochemical workstation (Shanghai Chen Hua CO. Ltd.). The preparation of specimen for photocurrent test and detailed experiment parameters are shown in supplementary information.

2.4 Photodegradation performance

Methylene blue (MB) was employed as the representative dye indicator to evaluate the UV photocatalytic activity of ZnO fibers. In a typical process, 0.1 g ZnO fibers heat-treated at different temperatures were immersed into 100 ml MB aqueous solution (20 mg/L) which was loaded in an open beaker. The solution was placed at a dark environment for 1 h to attain the absorption/desorption equilibrium. The mixture were then irradiated by a Xe lampe (300W), and the whole photocatalytic reaction took place at room temperature. UV-Vis absorption spectra of samples were measured at regular intervals to monitor the reaction, and the absorption at 660 nm was recorded as a function of irradiation time. A reference was made simultaneously using ZnO powders instead of fibers, and other experiment parameters stay the same.

3. Results and discussion

3.1 Formation of precursors

To find out the optimal condition for best spinnability (the spinnability was evaluated by inserting a glass rod into the viscous sol and pulling out to check whether a dry and continuous fiber can be obtained), a series of tests were performed by changing the molar ratio of CA to metal ions and pH values. The results are shown in Table 1. Correspondingly, the zinc citrate (ZC) complex formed in the aqueous solution under different conditions were also listed according to a potentiometric study.[26] As can be seen from the table, the optimal spinning performance was achieved at sample 6, which molar ratio was 1:1 with pH to be 5.8. The spinnability was highly related to the molecular structure of the ZC complex. When the species in precursor solution were single ligand zinc citrate (SL-ZC) complexes ($[Zn(cit)]^-$ and/or $[Zn(Hcit)]$), the obtained sol after concentration of the precursor solution was transparent and spinnable. Whereas, crystalline precipitate was obtained in the samples which the precursor solution contained double ligand zinc citrate (DB-ZC) complex ($[Zn(cit)_2]^{4-}$) or ZC dimer ($[Zn_2(cit)_2H_{-2}]^{4-}$). Obviously, these precipitate was not suitable for spinning.

Theoretical calculation[27] and extend X-ray absorption study[28] have demonstrated that possible configuration of SL-ZC complex is Zn^{2+} octahedrally coordinates to three carboxyl groups of one citric acid and three water molecules. In the research, ^{13}C-NMR spectra of sample 6 in solution were conducted to confirm the molecular structure further. As shown in Figure 1, in the precursor solution, the β-carbon of citrate resonates at 178.52 ppm, whereas the uncoordinated β-carbon of CA gives a signal at 173.40 ppm. The α-carbon of citrate in the precursor resonates at 176.77 ppm, showing a downfield shift compared to the free ligand (181.29 ppm). The carbon attached to hydroxyl group gives signal at 74.98 ppm in precursor solution, and the one in CA lies at 73.27 ppm. $-CH_2-$ group in precursor solution and CA has been observed at 44.12 and 43.27 ppm, respectively. In brief, the NMR peaks for the carbon atoms of carboxyl groups in precursor have a large shift whereas those for other two kinds of carbon atoms show almost the same behavior compared to free molecule of CA. The spectral feature reveals the involvement of all carboxyl groups in complexation and uncoordination of hydroxyl group.

Table 1. Effect of citric acid to Zn^{2+} ratio and pH value on spinnability.

NO.	CA:Zn^{2+} (mol ratio)	pH	Main species of zinc citrate complex*	Spinnability **
1	2:1	2.7	$[Zn(Hcit)]$, $[Zn(cit)]^-$	++
2	2:1	3.4	$[Zn(Hcit)]$, $[Zn(cit)]^-$	++
3	2:1	6.9	$[Zn(cit)]^-$, $[Zn(cit)_2]^{4-}$	-
4	2:1	9.2	$[Zn(cit)]^-$, $[Zn(cit)_2]^{4-}$, $[Zn_2(cit)_2H_{-2}]^{4-}$	-
5	1:1	3.2	$[Zn(Hcit)]$, $[Zn(cit)]^-$	+
6	1:1	5.8	$[Zn(cit)]^-$	+++
7	1:1	7.5	$[Zn_2(cit)_2H_{-2}]^{4-}$, [Zn(cit)]-	-
8	1:1	8.8	$[Zn_2(cit)_2H_{-2}]^{4-}$	-

* It is a general notation that not considering the molecules structures of the complex. In alkaline environment, negative value in $[Zn_2(cit)_2H_{-2}]^{4-}$ indicated the coordination of OH^- to Zn^{2+}.[26]

** The minus sign indicates the sample has no spinnability. The plus sign indicates the sample has spinnability, and the more sign, the better spinnability.

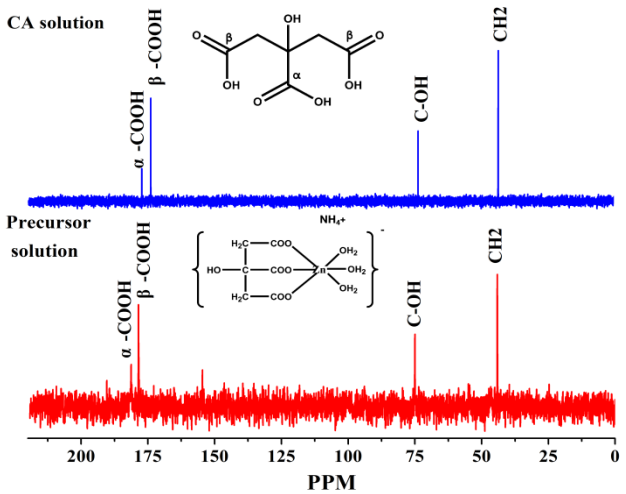

Figure 1. ^{13}C-NMR of CA and precursor solution

IR spectra of the spinnable gel precursors were investigated and are shown in Figure 2. The most relevant vibrations of CA are the $\nu_{(O-H)}$ of the α-hydroxyl at 3293 cm^{-1}, and the $\nu_{(C=O)}$ of the carboxylic groups at 1750-1700 cm^{-1}. In the spectra of gel precursors, the sharp absorption peak of $\nu_{(O-H)}$ was vanished and displaced by a broad band around 3300-3100 cm^{-1}. It is maybe caused by the interaction between α-hydroxyl and Zn^{2+}. Absorption peak of the $\nu_{(C=O)}$ ascribed to α-carboxyl was disappeared firstly with pH value increasing, indicating the central carboxyl group preferentially deproton due to high polarity which origins from the attraction of adjacent α-hydroxyl. The intensity of the absorption peaks of the $\nu_{(C=O)}$ ascribed to two equal β-carboxyl decreased as the pH value increases. Character doublet peaks ranging from 1200-1700 cm^{-1} ascribed to the asymmetric, and symmetric stretching vibration of COO- was arose simultaneously. The frequency differences between $\nu_{as(OCO)}$ and $\nu_{s(OCO)}$ offer the most sensitive indication of the mode of carboxylate coordination.[29, 30] In low pH values (sample 1, 2, 5), the frequency differences between them were above 200 cm^{-1} suggesting the monodentate which a carboxyl group only chelating the Zn^{2+}. In nearly neutral sample (sample 6), the value was 173 cm^{-1} indicating the bridging coordination which a carboxyl group coordinates a Zn^{2+} and a NH_4^+

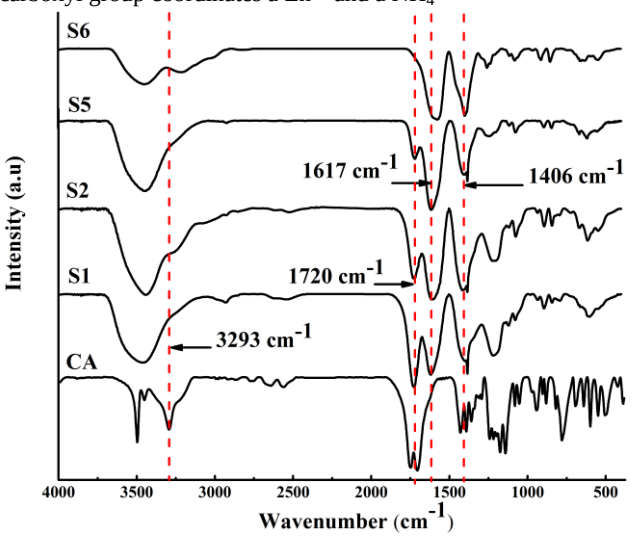

Figure 2. IR spectra of spinnable sample precursors

On the basis of above results, polymerization path of the ZC monomers occured in the process of concentration was proposed. In $[Zn(cit)]^-$ and [Zn(Hcit)], the flexibility of CA molecule allows three carboxyl of one CA coordinate to a Zn^{2+}. The hydroxyl is uncoordinated. The Zn^{2+} bonds to three water molecules to accomplish coordination. As the concentration proceeded, the solvent was evaporated and the monomers were closed to each other. The uncoordinated hydroxyl group attacks the Zn^{2+} of another SL-ZC monomer. Since the water molecule is a typical cleavage group, the nucleophilic substitution can thermodynamically occur. As the reaction proceed, the ZC monomers were assembled into a multinuclear molecule, and it has been reported[31] that an analogous multinuclear organozinc structure would form oil-like substance when vacuum evaporating the precursor solution. That was consistent with the phenomenon found in our research. Herein, it was deemed that the high viscosity of the distillation results from the interaction

between the multinuclear clusters. A simple schematic is shown in Schema 1. Although there is no data to describe the structure of the DL-ZC monomer in aqueous solution, it can learn from the crystal structure of a zinc citrate compound[32] that in DL-ZC monomer, the Zn^{2+} is fully surrounded by two CA molecules. In ZC dimer, due to the alkaline condition, the aquo ligand (H_2O) of the SL-ZC monomer hydrolyzed into hydroxo ligand (-OH),[33] such hydroxo-metal monomers have tendency to bridge to each other via olation. The possible configuration of the two molecule structures were listed in Schema 1. From the figure, it can be deduced that the polymerization process can not occur due to the higher electronegativity of the ligands (citric acid and hydroxyl group) retarding the abovementioned nucleophilic substitution. To decrease the total energy of the system, each unit arranges into ordered crystalline structure when the precursor solution was evaporation.

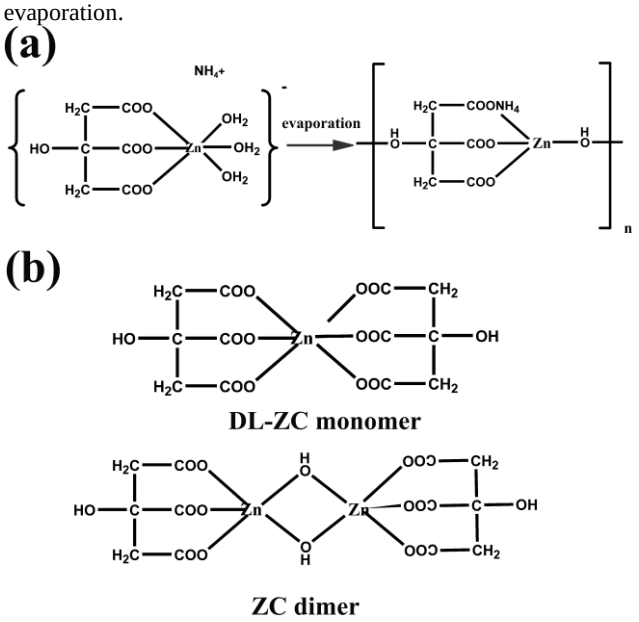

Schema 1. (a) Schematic of the polymerization process of SL-ZC monomers inducing by evaporation; (b) the molecular structure of the DL-ZC monomer and ZC dimer

3.2 Thermal decomposition of precursors

The TG/DSC analyses of the gel precursors，the IR spectra and XRD patterns of the gel fibers heat-treated at different temperatures were used to investigate the transformation process of the precursors in detail (Figure 3). The decomposition of the precursors possesses four steps distinguished by thermal analysis. In the first step, beneath 200 ℃, the weight loss of about 5 % is mainly due to the decomposition of carboxylic amides accompanied with ammonia gas release.[34] As a result, the IR spectra clearly features some free acid carboxylic groups at 1720 cm^{-1}, which is the product of the above reaction. In the second decomposition region, from 200 to 300 ℃, an evident endothermic peak can be observed at 224 ℃, which comes from dehydroxylation of the α-hydroxyl in CA. Correspondingly, the absorption peak of IR spectra at 3213 cm^{-1} ascribed to stretch vibration of α-hydroxyl was vanished. The weight loss of 12.69 % after the dehydroxylation was well fitted with the total weight of NH_3 and H_2O. Meantime, the dehydroxylation leads to the formation of ethylene linkage. Owing to the generated conjugative effect between carbon double bond and carboxyl group, a new peak at 1780 cm^{-1} arose. In the next stage, ranges from 300 to 400 ℃, an exothermal peak located at 380 ℃ is the crystallization of ZnO, and the IR vibration of ZnO was detected at 480 cm^{-1}. With the dehydroxylation and subsequent decarboxylation of the zinc citrate complex, the Zn^{2+} gets decoordinated by its ligand and ZnO is formed. At last stage, an exothermal peak at 460 ℃ indicates that the residual organics were decomposed accompanying with violent combustion reaction. After decomposition, the remaining weight percentage at 500 ℃ is 31.59 %, which was in accordance with the theoretical value of 29.75 % for ZnO. As shown in XRD patterns, The fibers were still amorphous even when the treatment temperature was 350 ℃. The characteristic peaks of ZnO were observed after heat treatment at 400 ℃. It was consistent with the results obtained by thermal analysis and IR spectra where the crystallization exothermic peak located at about 380 ℃ and the IR absorption peaks of ZnO were detected in the sample heat treated at 400 ℃. The patterns were well fitted to JCPDS 36-1451. A schematic of decomposition process is shown in Schema 2.

Generally, dehydroxylation and decarboxylation occur at 145 and 225 ℃ in CA, respectively.[34] However, in our research, dehydroxylation occurred above 200 ℃ and the decarboxylation finished at 400 ℃. Such a difference in decomposition process was also the evidence that all function groups in CA are involved in coordination which is the origin of the formation of multinuclear structure.

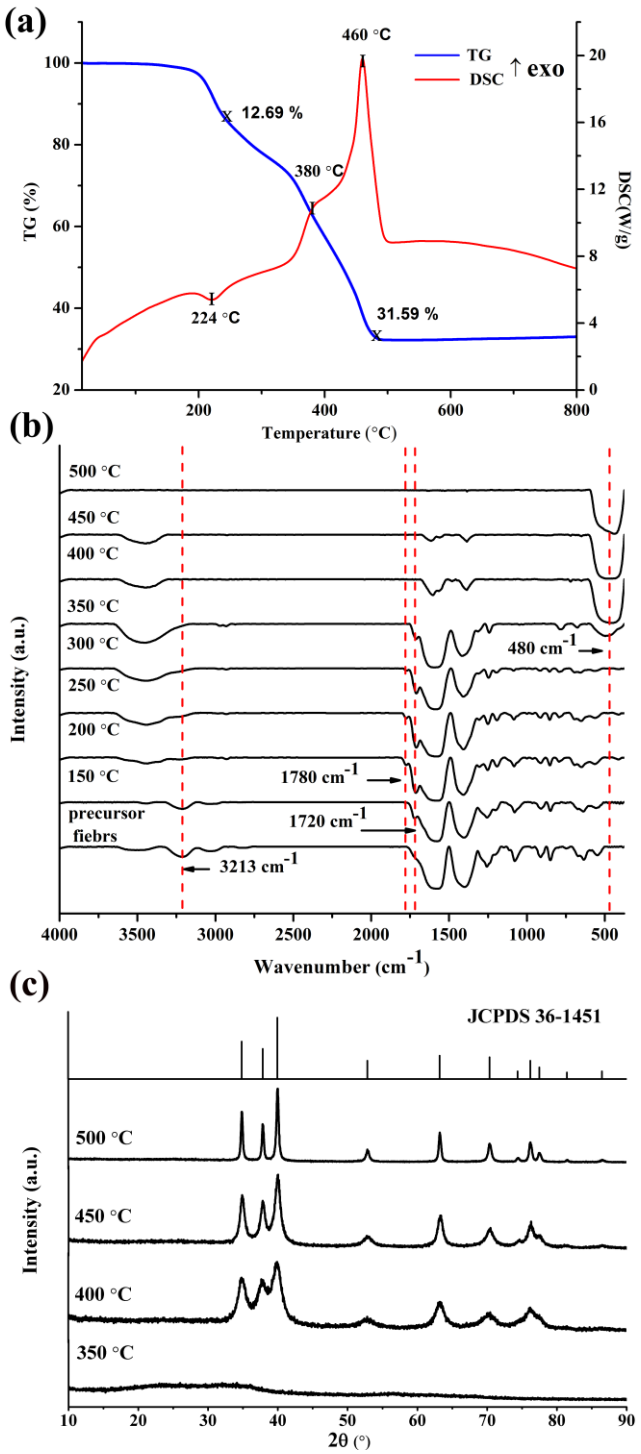

Figure 3. (a) TG/DSC analyses of gel precursors, (b) IR spectra and (c) XRD patterns of the gel fibers heat-treated at different temperatures.

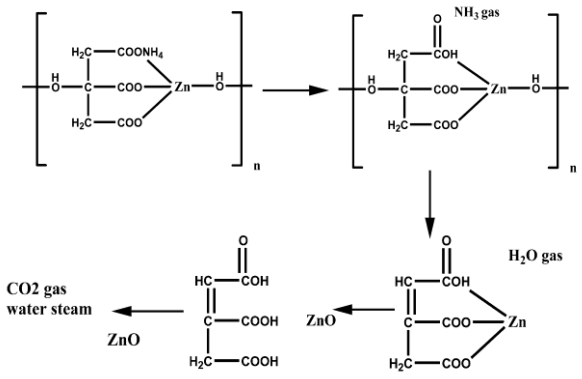

Schema 2. Schematic of the decomposition process for gel precursors

3.3 Crystallization and microstructure of ZnO fibers.

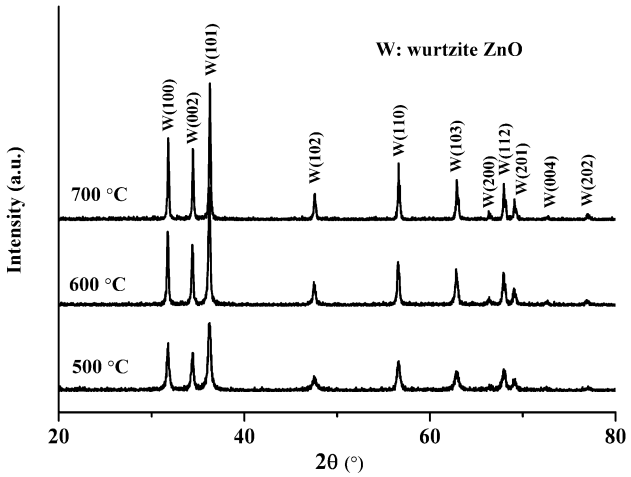

Figure 4. XRD patterns of the fibers heat-treated at different temperature.

Figure 4 shows the XRD patterns of the fibers heat-treated at different temperatures. The obtained fibers were wurtzite phase with exposing their characteristic crystal faces. As the temperature increases, the diffraction peaks of the fibers become sharp due to crystal growth. Figure 5 displays the digital images of the fibers heat-treated at 500 ℃ and the microstructures of the as received ZnO fibers heat-treated at different temperatures. Micrographs seen from the figures, high quality ZnO fibers can be fabricated in large scales. After heat treatment, the samples remained in fiber form with the length of about 5 mm (Figure S2). The diameter of precursor fibers was about 5 μm and became 3 μm for the fibers heat-treated at 700 ℃ because of the removal of organics (Figure S2). After thermal decomposition, the section of the fibers was poly-porous due to gas release which results from decomposition of organics. Yan[35] has also found that the gas is a soft template in the synthesis of porous ZnO materials. As the temperature increases, the crystal growth makes the fibers more compacted. From the surface of the fibers, it can be seen that the fibers were composed of nanoparticles. The grain size was increased with the temperature increasing, after heat treatment at 700 ℃, the grain size of the particles was about 100 nm, and the morphology was close to prismatic that is consistent with the idealized growth habit of ZnO crystal.[36]

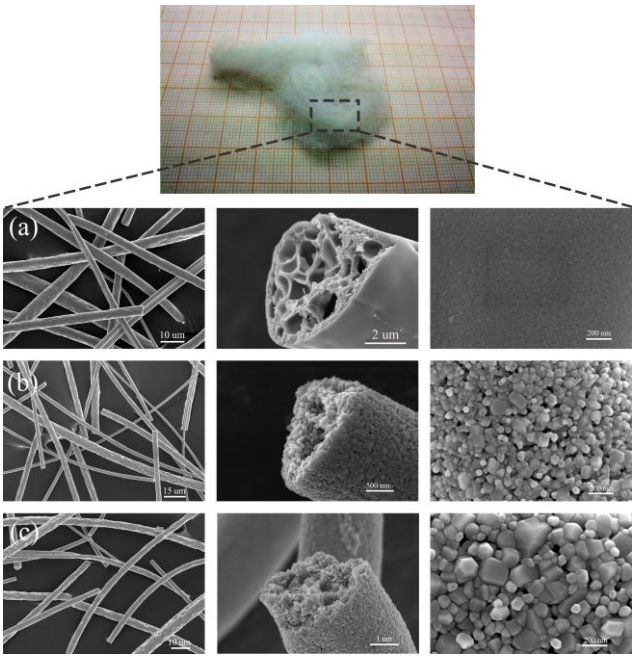

Figure 5. Digital image of the product fibers heat treated at 500 ℃ (top), SEM images of the fibers heat treated at (a) 500 ℃, (b) 600 ℃, (c) 700 ℃ (bottom).

3.4 Photodegardation performance

Figure S3 shows the UV-Vis spectra recorded during the photocatalytic degradation of MB and Figure 6 shows the results of photodegradation investigation. As can be seen from the figures, the fibers heat-treated at 600 ℃ have better degradation performance than ZnO powders. With the photocatalytic ability of ZnO, the blue dye can transform into almost colorless solution through long time radiation. The fluffy fibers immersed in solution were contacted with target reactant sufficiently without stirring. After the degradation, the fibers were still self-standing in the reaction vessel, which would be good for isolation or employment in continuous reaction system. Without stirring, the ZnO powders were deposited on the bottom of the beaker. it would decrease the contact between reactant and catalysts. The photocurrent and BET surface area of fibers and powders were measured (shown in Figure S3 and Table S2). From the figure and table, it demonstrated that the fibers heat-treated at 600 ℃ have higher photocurrent response than powders and other fibers sample. It is considered that the highly crystalline and closely interconnected nanoparticles in fibers are beneficial for the vectorial transfer of photoinduced charge carriers through the grain boundaries, leading to the high separation efficiency of electron-hole pairs[18]. Although its surface area is less than powders and fibers heat-treated at 500 ℃, it has the best photocatalytic activity. It maybe derived from the best photocurrent response and sufficient contact with reactant which increases the activity sites.

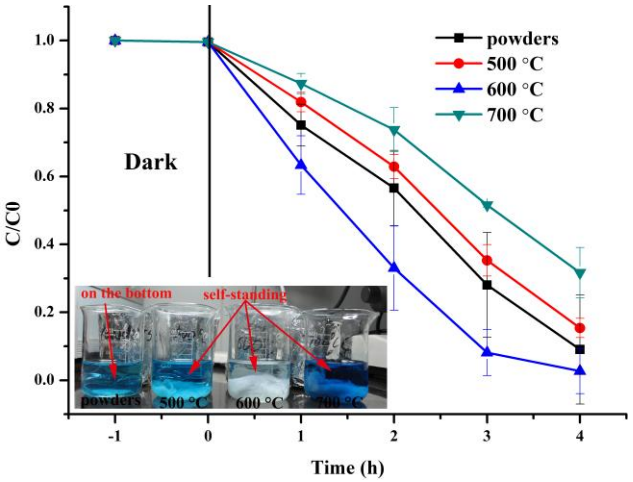

Figure 6. Photocatalytic activity comparison between the fibers and powders

4. Conclusions

Robust ZnO fibers have been fabricated by centrifugal-spinning a organozinc sol into gel fibers followed by heat treatment. Cheaper and environmental friendly starting materials, ZnO powders and citric acid, were used. Through a series of characterizations on precursor sol and gel fiebrs, it was found that zinc citrate monomers in the precursor solution were assembled into multinuclear molecule induced by solvent evaporation. The assembling is nucleophilic substitution of uncoordinated hydroxyl groups of citric acid to metal ions. Due to the interaction between the multinuclear clusters, the precursor solution maintained stable amorphous state with high viscosity. We believe that, the investigation on the polymerization of metal citrate complex can inspire peer researchers to design new functional materials (coating, fiber, etc.) through this process. As a solid catalysts, the as prepared ZnO fibers have advantages that self-standing in reaction, sufficiently contact with reactant, and easy be recycled compared to their powder counterparts. It has potential applications in the synthesis of chemical energy, such as biodiesel, alcohol fuel as well as photo-assistant eliminating environmental pollution.

Acknowledgements

The authors thank the National Natural Science Foundations of China (Grant Nos. 51102155 and 51372140), the Research Fund for the Doctoral Program of Higher Education (RFDP, 20110131120018), and the Youth Scientist Fund of Shandong Province (BS2011CL025) for financial support.

Notes and references

State Key Laboratory of Crystal Materials and Institute of Crystal Materials, Shandong University, Jinan 250100, PR China.
Tel: +86 53188362776.
E-mail: zhuly@sdu.edu.cn (Luyi Zhu), xdoffice@sdu.edu.cn (Dong Xu)

†Electronic Supplementary Information (ESI) available: Digital images and parameters table of centrifugal-spinning process. Figures of fiber length and diameter measurements. UV-Vis spectra recorded during the photocatalytic degradation of MB. Photocurrent and BET surface area of fibers and powders.

1 L. Y. Zhu, X. Q. Wang, G. H. Zhang, Q. Ren and D. Xu, Appl. Catal. B-Environ, 2011, 103, 428-435.
2 W. W. He, H. K. Kim, W. G. Wamer, D. Melka, J. H. Callahan and J. J. Yin, J. Am. Chem. Soc, 2014, 136, 750-757.
3 R. Madhuvilakku and S. Piraman, Bioresour Technol, 2013, 150, 55-59.
4 V. Montes, M. Checa, A. Marinas, M. Boutonnet, J. M. Marinas, F. J. Urbano, S. Järas and C. Pinel, Catal. Today., 2014, 223, 129-137.
5 S. Banerjee and A. Saha, New J. Chem, 2013, 37, 4170-4175.
6 Y. T. Zhi, D. W. Y. Yong, Z. H. Zhang, H. Y. Low, L. W. Chen and W. S. Chin, J. Phys. Chem. C, 2013, 117, 10780-10787.
7 Z. Shami and N. Sharifi-Sanjani, Cryst. Eng. Comm, 2014, 16, 910.
8 M. A. Behnajady, N. Modirshahla, N.Daneshvar, M. Rabbani, J. Hazard. Mater, 2007, 140, 257-263.
9 F. Nobrega, A. Polo, A. Benedetti, M. Leao, V. Santana and N. Machado, J.Hazard. Mater, 2013, 263P, 61-66.
10 X. H. Yang, C. L. Shao, H. Y. Guan, X. L. Li and J. Gong, Inorg. Chem. Comm, 2004, 7, 176-178.
11 R. Siddheswaran, R. Sankar, M. Ramesh Babu, M. Rathnakumari, R. Jayavel, P. Murugakoothan and P. Sureshkumar, Cryst. Res. Technol, 2006, 41, 446-449.
12 D. D. Lin, W. Pan and H. Wu, J. Am. Ceram. Soc, 2007, 90, 71-76.
13 D. D. Lin, H. Wu, R. Zhang and W. Pan, Chem. Mater, 2009, 21, 3479-3484.
14 Z. Y. Zhang, C. L. Shao, X. H. Li, C. H. Wang, M. Y. Zhang and Y. C. Liu, ACS Appl. Mater. Inter, 2010, 2, 2915-23.
15 A. J. Turinske, S. A. Nelson, N. Stojilovic. S. B. Ali, V. S. Dordevic, E. A. Evans, J. Sol-Gel. Sci. Tech, 2012, 65, 283-286.
16 S. S. Mali, H. Kim, W. Y. Jang, H. S. Park, P. S. Patil and C. K. Hong, ACS Sustainable Chemistry & Engineering, 2013, 1, 1207-1213.
17 P. Singh, K. Mondal and A. Sharma, J. Colloid. Interface. Sci, 2013, 394, 208-215.
18 S. K. Choi, S. Kim, S. K. Lim and H. Park, J. Phys. Chem. C., 2010, 114, 16475-16480.
19 D. Schawaller, B. Clauß and M. R. Buchmeiser, Macromol. Mater. Eng, 2012, 297, 502-522.
20 S. Padron, A. Fuentes, D. Caruntu, and K. Lozano, J. Appl. Phys, 2013, 113, 024318.
21 C. Y. Zhang, X. Q. Shen, J. X. Zhou, M. X. Jing and K. Cao, J. Sol-Gel. Sci. Tech, 2007, 42, 95-100.
22 F. Z. Song, X. Q. Shen, M. Q. Liu and J. Xiang. Solid. State. Sci, 2010, 12, 1603-1607.
23 X. Q. Shen, Z. Zhou, F. Z. Song and X. F. Meng, J. Sol-Gel. Sci. Tech, 2009, 53, 405-411.
24 L. Lin, H. Y. Cui, G. H. Zeng, M. L. Chen, H. F. Xu, X. Q. Shen, C. Bortolini and M. D. Dong, J. Mater. Chem. B, 2013, 1, 2719.
25 L. Lin, S. Vittayapadung, X, Q. Li, W. W. Jiang and X. Q. Shen, Environ. Prog. Sustain. Energy, 2013, 32, 1255-1261.
26 S. Capone, A. D. Robertis, C. D. Stefano and S. Sammartano, Talanta, 1986, 33, 763-767.
27 J. R. Black, A. Kavner and E. A. Schauble, Geochim. Cosmochim. Ac, 2011, 75, 769-783.
28 D. E. Salt, R. C. Prince, A. J. M. Baker, I. Raskin and I. J. Pickering, Environ. Sci. Technol, 1999, 33, 713-717.
29 K. Nakamoto, J. Fujita, S. Tanaka and M. Kobayashi, J. Am. Chem. Soc, 1957, 79, 4904-4908.
30 M. Nara, H. Torii and M. Tasumi, J. Phys. Chem, 1996, 100, 19812-198817.
31 R. C. Hoffmann, and J. J. Schneider, Eur. J. Inorg. Chem, 2014, 2241-2247.
32 R. Swanson, W. Ilsley and A. Stanislowski, J. Inorgan. Biochem, 1983, 18, 187-194.
33 J. Livage, M. Henry and C. Sanchez, Prog. Soild. St. Chem, 1988, 18, 259-341.
34 K. V. Van Werde, D. Mondelaers, G. Vanhoyland, D. Nelis, M. K. Van Bael, J. Mullens and L. C. Van Poucke, J. Mater. Sci, 2002, 37.
35 S. Cheng, D. Yan, J. T. Chen, R. F. Zhou, J. J. Feng, H. J. Li, H. T. Feng, and P. X. Yan, J. Phys. Chem, 2009, 113, 13630-13635.
36 W. J. Li, E. W. Shi, W. Z. Zhong and Z. W. Yin, J. Cryst. Growth, 1999, 203, 186-196.

TOC

For easy recycling and a better application in continuous mode in catalytic reactions, fiberous ZnO were fabricated.